JACS
JOURNAL OF THE AMERICAN CHEMICAL SOCIETY
Article
pubs.acs.org/JACS

Hyperbranched Self-Immolative Polymers (*h*SIPs) for Programmed Payload Delivery and Ultrasensitive Detection

Guhuan Liu,[†] Guofeng Zhang,[†,‡] Jinming Hu,[†] Xiaorui Wang,[†] Mingqiang Zhu,[‡] and Shiyong Liu*[,†]

[†]CAS Key Laboratory of Soft Matter Chemistry, Hefei National Laboratory for Physical Sciences at the Microscale, *i*Chem (Collaborative Innovation Center of Chemistry for Energy Materials), Department of Polymer Science and Engineering, University of Science and Technology of China, Hefei, Anhui 230026, China

[‡]Wuhan National Laboratory for Optoelectronics, College of Chemistry and Chemical Engineering, Huazhong University of Science and Technology, Wuhan, Hubei 430074, China

Supporting Information

ABSTRACT: Upon stimuli-triggered single cleavage of capping moieties at the focal point and chain terminal, self-immolative dendrimers (SIDs) and linear self-immolative polymers (*l*-SIPs) undergo spontaneous domino-like radial fragmentation and cascade head-to-tail depolymerization, respectively. The nature of response selectivity and signal amplification has rendered them a unique type of stimuli-responsive materials. Moreover, novel design principles are required for further advancement in the field of self-immolative polymers (SIPs). Herein, we report the facile fabrication of water-dispersible SIPs with a new chain topology, hyperbranched self-immolative polymers (*h*SIPs), by utilizing one-pot AB_2 polycondensation methodology and sequential postfunctionalization. The modular engineering of three categories of branching scaffolds, three types of stimuli-cleavable capping moieties at the focal point, and seven different types of peripheral functional groups and polymeric building blocks affords both structurally and functionally diverse *h*SIPs with chemically tunable amplified-release features. On the basis of the *h*SIP platform, we explored myriad functions including visible light-triggered intracellular release of peripheral conjugated drugs in a targeted and spatiotemporally controlled fashion, intracellular delivery and cytoplasmic reductive milieu-triggered plasmid DNA release via on/off multivalency switching, mitochondria-targeted fluorescent sensing of H_2O_2 with a detection limit down to ~20 nM, and colorimetric H_2O_2 assay via triggered dispersion of gold nanoparticle aggregates. To further demonstrate the potency and generality of the *h*SIP platform, we further configure it into biosensor design for the ultrasensitive detection of pathologically relevant antigens (e.g., human carcinoembryonic antigen) by integrating with enzyme-mediated cycle amplification with positive feedback and enzyme-linked immunosorbent assay (ELISA).

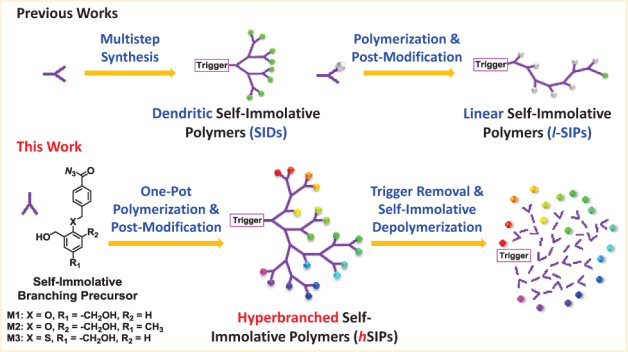

INTRODUCTION

Biological systems can sense and respond to exogenous and endogenous signals through well-ordered multiple molecular events to achieve signal transduction and amplification.[1] The long-standing pursuits of mimicking intricate processes and functions intrinsic of living organisms[2] have spurred the development of stimuli-responsive polymeric materials.[3] Current challenges in this emerging field include achieving sophisticated structural and sequence control, establishing advanced biomimetic functions, and fabricating more sensitive and selective systems.[4] The latter relies on the integration with chemical and biochemical amplification strategies. In this context, enzyme-mediated catalytic reactions, which are closely relevant to amplification detection techniques such as polymerase chain reaction (PCR) and enzyme-linked immunosorbent assay (ELISA), have led to responsive polymers with improved sensitivity, selectivity, and specificity.[5] However, the multimolecular nature of these enzyme-involved systems renders largely compromised signal amplification performance in highly complex biological milieu.[1] On the other hand, responsive polymers exhibiting input signal amplification features at a unimolecular level are nonconventional, with self-immolative dendrimers (SIDs)[6] and linear self-immolative polymers (*l*-SIPs)[7] being rare examples of this type.

Originally proposed in 2003,[6a−c] SIDs can undergo spontaneous domino-like radial fragmentation upon triggered cleavage of a single capping moiety at the focal point. The release of peripheral functional groups allows for exponential signal amplification with the extent depending on the generation of SIDs. This feature as well as advantages including programmed fragmentation and tunable multivalency[8] have promoted the construction of advanced drug/gene delivery and diagnostic functions, mostly in aqueous media.[6] However, SIDs

Received: May 15, 2015
Published: September 1, 2015

DOI: 10.1021/jacs.5b05060
J. Am. Chem. Soc. 2015, 137, 11645−11655

suffer from challenging multistep synthesis and tedious purification procedures (Scheme 1).[9]

Scheme 1. Schematic Illustration of Hyperbranched Self-Immolative Polymers (*h*SIPs), Which Represent a New Chain Topology in the Field of Self-Immolative Polymers Exhibiting Triggered Cascade Depolymerization Characteristics[a]

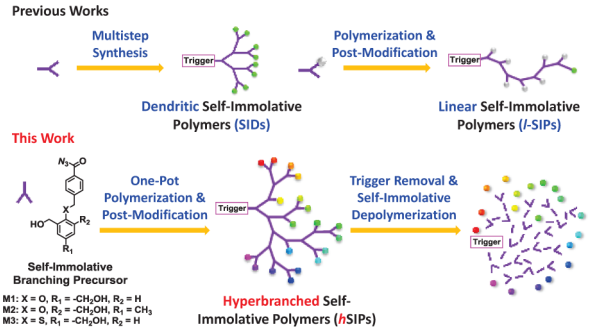

[a]For clarity, schematic structures of conventional SIDs and *l*-SIPs are also shown. Upon stimuli-triggered cleavage of capping moiety at the focal point, self-immolative depolymerization of *h*SIPs releases multiple bioactive agents initially conjugated at the periphery, as well as small molecule branching units.

The invention of the concept of *l*-SIPs later in 2008 by Shabat et al.[7a] can partially solve the above issues as the synthesis of *l*-SIPs can be conducted in one-pot via either polycondensation[10] or chain growth approaches.[11] Note that functional reporters in *l*-SIPs can be either installed at the distal end or conjugated as side moieties. In the former case, no signal amplification can be achieved, whereas in the latter case, triggered cleavage of capping terminal moiety will release multiple functional moieties with the extent of amplification dictated by the chain length (Scheme 1). However, *l*-SIPs equipped with side chain release motifs are also synthetically challenging,[7a,12] and thus most of the reported *l*-SIPs have not utilized this feature to achieve functional amplification.[7] As compared to those of SIDs,[6] core functions of *l*-SIPs in aqueous media (e.g., amplified drug delivery and sensing) have been far less explored.[7] Few existing examples are based on *l*-SIPs in the form of the molecularly dissolved state[7a,12] or colloidal dispersions.[10a−c,11d,e,13]

The current status of both SIDs and *l*-SIPs revealed that it has remained a considerable challenge to fabricate self-immolative polymers (SIPs) with facile synthesis, high chemical amplification potency, modular design, and multifunctional integration. Further advancement in the field of SIPs thus requires the introduction of novel design criteria. It is well-known that, besides linear, cyclic, star, and dendritic polymers, hyperbranched polymers (HBPs) represent an unique type of chain topology possessing highly branched and three-dimensional globular architecture. HBPs can be readily synthesized via one-pot polymerization of AB_X monomers[14] or inimers/comonomers.[15] Despite being less structurally uniform than dendrimers, HBPs are distinguished by a large number of peripheral terminal moieties, which can be facilely functionalized (e.g., drugs and fluorophores) for drug/gene delivery, optical sensing, and theranostic applications.[16] Our previous interest in responsive polymers with self-immolative motifs (building blocks[13] and side linkages[17]) and hyperbranched polymers with self-immolative drug comonomers[18] has prompted us to speculate the possibility of fabricating hyperbranched self-immolative polymers (*h*SIPs). Theoretically, *h*SIPs are expected to not only inherit advantages of conventional HBPs such as facile synthesis, modular design, and multifunctionalization, but also possess potent chemical amplification and programmed release characteristics (Scheme 1).

Herein, we report on the facile fabrication of SIPs with a hyperbranched chain topology. The general design principle of *h*SIPs is shown in Scheme 2. Starting from three categories of AB_2-type branching precursors (**M1**, **M2**, and **M3**), one-pot polycondensation reaction and subsequent caging reactions with three types of capping moieties (responsive to visible light, H_2O_2, and intracellular reductive milieu, respectively) at the focal point afford a series of *h*SIP scaffolds with chemically tunable depolymerization rates and varying responsive modes. The structural and functional diversity of *h*SIPs could be further expanded through rich choices of functionalization at the periphery. On the basis of the *h*SIP platform, we construct myriad functions including visible light-triggered spatiotemporal and intracellular delivery of peripheral conjugated drugs, intracellular delivery and cytoplasmic reductive milieu-triggered plasmid DNA release via on/off multivalency modulation, mitochondria-targeted fluorescent sensing of H_2O_2 with enhanced detection limit, and colorimetric H_2O_2 assay via triggered dispersion of gold nanoparticle aggregates. We also configure *h*SIPs into biosensor design for the ultrasensitive detection of pathologically indicative antigens by integrating with enzyme-mediated cycle amplification and ELISA technique.

RESULTS AND DISCUSSION

Modular Synthesis of *h*SIPs. Inspired by the pioneering work of Shabat et al.[7a] concerning *l*-SIPs and relevant literature reports,[12a,19] our initial design of *h*SIPs involves the use of trifunctional benzene derivatives with one caged isocyanate and two hydroxyl-containing moieties at *ortho* and *para* positions by learning the principle developed by Frechet et al.[14d] for the synthesis of conventional HBPs. 2,4-Bis(hydroxymethyl)aniline derivative is prone to intramolecular cyclization with 6-membered ring formation during branching polycondensation. On the other hand, choosing 2-(3-hydroxy-1-propenyl)-4-hydroxymethylaniline derivative as latent precursor involves multistep synthesis with unsatisfactory overall yield, and the final *h*SIP scaffold is poorly water-dispersible.[20] The limited success of these initial trials prompted us to explore alternate design approaches for *h*SIPs. We recently developed the idea that bridging the caged isocyanate moiety with two reactive hydroxyl functionalities through self-immolative linkages might endow AB_2 polycondensation precursors with improved structural stability and better synthetic access (Schemes 1 and 2).

M1−M3 branching precursors with varying hydroxymethyl substituting positions and activatable linkages (O or S) were then designed to achieve chemically tunable depolymerization rates for the *h*SIP scaffolds (Scheme S1, Figures S1−S3). The hyperbranched scaffolds of *h*SIPs (***h*SIP1**-***h*SIP10**) were synthesized through polycondensation of **M1**, **M2**, or **M3** AB_2-type precursors (Scheme 2) at 110 °C.[7a,14d] The polycondensation reactions were quenched by reacting with three types of capping agents including perylen-3-yl methanol (*per*), hydroxymethyl phenylboronic ester (*PB*), and diethanol disulfide (*SS*); this process introduced responsiveness of

DOI: 10.1021/jacs.5b05060
J. Am. Chem. Soc. 2015, 137, 11645−11655

Scheme 2. Reaction Schemes Employed for the Synthesis and Functionalization of *h*SIPs Possessing Three Categories of Branching Scaffolds (M1−M3) and Three Types of Capping Moieties at the Focal Point Which Are Responsive to Visible Light (Perylen-3-yl, *per*), H_2O_2 (Phenylboronic Ester, *PB*), and Intracellular Reductive Milieu (Disulfide, *SS*), with Inert Benzyl (*Bn*) Capping Functionality Serving as a Control[a]

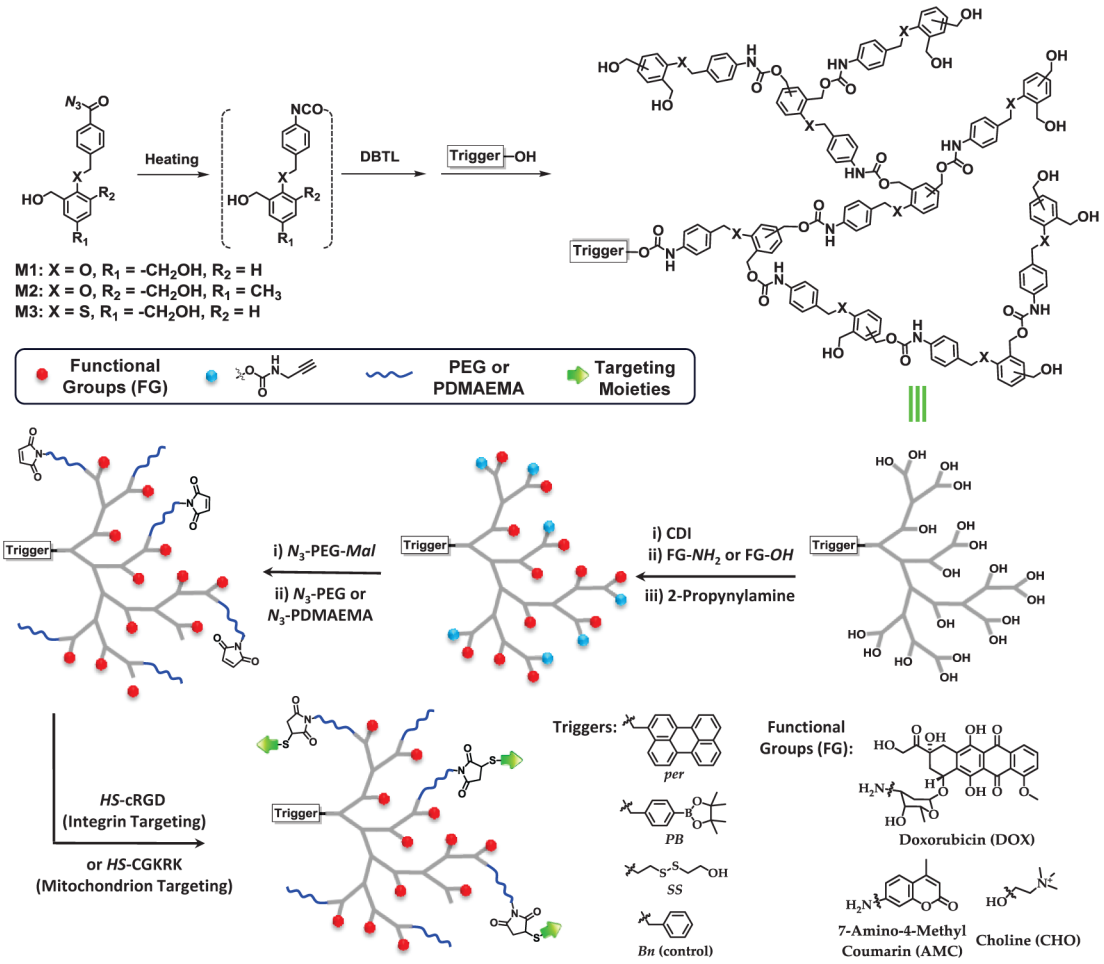

[a]A variety of bioactive and structural agents are conjugated at the periphery of *h*SIPs for specific functions including chemotherapy (doxorubicin, DOX), fluorescent sensing (caged coumarin, AMC), enzymatic reaction substrate for signal amplification (choline, CHO), triggered elimination of multivalent interactions with negatively charged species such as plasmid DNA and gold nanoparticles (PDMAEMA block, CHO), cell membrane or mitochondrion targeting (*HS*-cRGD or *HS*-CGKRK), and dispersibility of *h*SIPs in aqueous media (PEG).

Table 1. Structural Parameters of Hyperbranched Self-Immolative Polymers (*h*SIPs) Synthesized in This Work

entry	branching units	capping moieties	total no. terminal units[a,b]	functional groups (FGs)	N_{FG}[a]	functional polymer (FP)	N_{FP}[a]	targeting moieties	$M_{n,MALS}$ (kDa)[c]	M_w/M_n[c]
*h*SIP1	M1	*per*	19	DOX	10	PEG_{45}	6.5	cRGD	30.5	1.66
*h*SIP2	M2	*per*	14	DOX	6	PEG_{45}	5.5	cRGD	25.4	1.82
*h*SIP3	M3	*per*	16	DOX	8	PEG_{45}	6	cRGD	28.6	1.73
*h*SIP4	M1	*SS*	16	DOX	8	PEG_{45}	5.5		26.3	1.89
*h*SIP5	M1	*SS*	16			$PDMAEMA_8$	13		29.3	1.76
*h*SIP6	M1	*Bn* control	17			$PDMAEMA_8$	11		27.8	1.69
*h*SIP7	M1	*PB*	18	AMC	9	PEG_{45}	5	CGKRK	27.3	1.88
*h*SIP8	M1	*PB*	18	AMC	9	PEG_{45}	5		27.3	1.88
*h*SIP9	M1	*PB*	18	CHO	16					
*h*SIP10	M1	*PB*	18	CHO/AMC	8/2.5	PEG_{45}	4.5			

[a]Calculated from ^{1}H NMR results. [b]Total number of peripheral functional moieties (including modified and unmodified hydroxymethyl residues) conjugated at the periphery of *h*SIP scaffolds. [c]Molecular weights, M_n's, and molecular weight distributions, M_w/M_n's, were evaluated by GPC/MALS using DMF as the eluent (1.0 mL/min).

capping moieties at the *h*SIP focal point toward visible light, H_2O_2, and cytoplasmic reductive milieu, respectively. Benzyl alcohol (*Bn*) was also utilized as an inert capping agent to serve as a control. The total number of terminal hydroxyl groups at the periphery of as-synthesized *h*SIP scaffolds were determined to be in the range 14−19 by ^{1}H NMR analysis (Table 1,

DOI: 10.1021/jacs.5b05060
J. Am. Chem. Soc. 2015, 137, 11645−11655

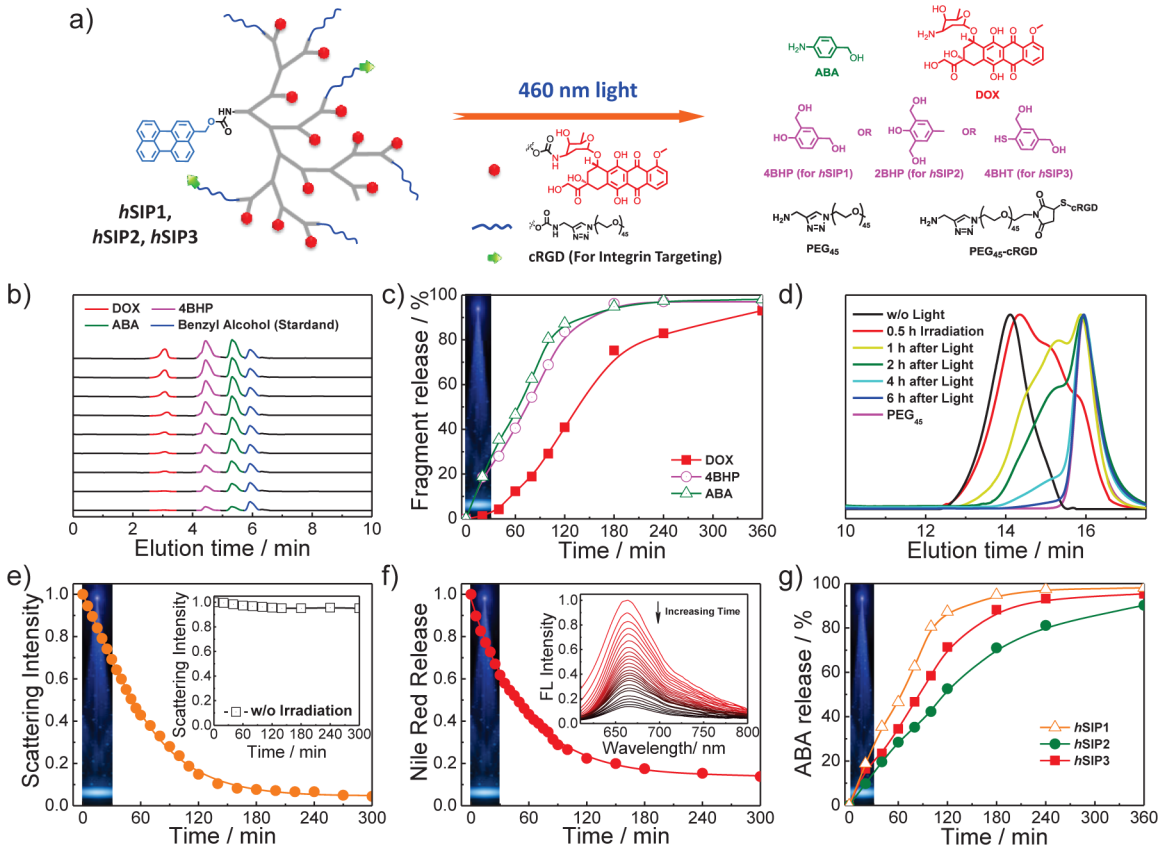

Figure 1. (a) Schematic illustration of self-immolative cascade depolymerization of ***h*SIP1**, ***h*SIP2**, and ***h*SIP3** triggered by 460 nm blue light irradiation. (b) HPLC traces (MeOH/H_2O 7/3 v/v; 260 nm absorbance; benzyl alcohol as an external standard) and (c) time-dependent evolution of the extent of spontaneous release of ABA, 4BHP, and DOX recorded for the aqueous solution of ***h*SIP1** (0.1 g/L, 25 °C) upon blue light irradiation for 30 min (blue region), followed by extended incubation under dark condition. (d) DMF GPC traces recorded for ***h*SIP1** without irradiation (black line) and upon incubating for 0 h (red line), 1 h (yellow line), 2 h (cyan line), 4 h (green line), and 6 h (blue line) after 30 min blue light irradiation. (e) Normalized scattering light intensities recorded for aqueous ***h*SIP1** solution upon 30 min blue light irradiation followed by extended incubation. (f) Nile red (NR) release profile from the hydrophobic core domains of ***h*SIP1**; the inset shows the evolution of fluorescence emission spectra (λ_{ex} = 550 nm) of NR. (g) *In vitro* release profiles of ABA from ***h*SIP1**, ***h*SIP2**, and ***h*SIP3** (0.1 g/L, 25 °C); the extent of spontaneous release of ABA was monitored by HPLC during 30 min blue light irradiation (blue region) and upon extended incubation under dark condition.

Figures S4–S6). When fully conjugated with releasable reporter molecules at the periphery, these *h*SIPs will exhibit signal amplification capability comparable to SIDs of the fourth generation, the synthesis of which has not been accomplished yet.[6] In addition, just as conventional hyperbranched polymers, as-prepared *h*SIPs are less branched and possess higher MWs compared to dendrimers with a similar number of peripheral functional groups.

Next, peripheral hydroxymethyl moieties of as-synthesized hyperbranched scaffolds with caging moieties at the focal point were activated by *N*,*N*′-carbonyldiimidazole (CDI) at first, and a variety of functional, bioactive, or structural agents including doxorubicin (DOX), 7-amino-4-methylcoumarin (AMC), choline (CHO), and propargylamine were conjugated. Finally, structural or functional hydrophilic segments such as poly(ethylene oxide) (PEO), poly(2-(dimethylamino)ethyl methacrylate) (PDMAEMA), and targeting peptides (intergrin-targeting cRGD peptide and mitochondrion-targeting CGKRK peptide) were covalently attached to the periphery through copper-catalyzed azide–alkyne cycloaddition (CuAAC) or thiol-maleimide click reactions, affording target *h*SIPs (***h*SIP1**–***h*SIP10**). All intermediate precursors and *h*SIPs were well-characterized by ^{1}H NMR, FT-IR, and GPC (Figures S4–S7). Structural parameters of all *h*SIPs are summarized in Table 1.

Visible Light-Triggered Spatiotemporal Intracellular Drug Delivery. With these functionalized *h*SIPs in hand, we first examined visible light responsiveness of ***h*SIP1**-***h*SIP3** with the same visible light-responsive capping moiety but different hyperbranched scaffolds (Figure 1a). Due to the presence of hydrophilic PEO segments (~6 per *h*SIP molecule), ***h*SIP1** can be directly dispersed into water and exists as relatively monodisperse spherical nanoparticles as evidenced by TEM and dynamic light scattering (DLS) measurements; the latter revealed an intensity-average hydrodynamic diameter, $\langle D_h \rangle$, of ~18 nm (Figure S8). After 30 min blue light irradiation at 460 nm to fully remove *per* capping moieties, the subsequent spontaneous self-immolative radial fragmentation of ***h*SIP1** was traced by GPC and HPLC via monitoring the concentrations of released small molecule ABA, 4BHP, and DOX drug (Figure 1b). A total of ~6 h was required for complete depolymerization of ***h*SIP1** (>95% DOX release, Figure 1c). The degradation process can be also monitored by the evolution of GPC traces, revealing a gradual decrease in molecular weights (MW) upon extending incubation duration (Figure 1d). Notably, the final MW of residual fragments was consistent with that of

DOI: 10.1021/jacs.5b05060
J. Am. Chem. Soc. 2015, 137, 11645–11655

peripheral PEO segments conjugated at the periphery of ***h*SIP1** (M_n ~ 2 kDa) (Figure 1d). This confirmed complete disintegration of ***h*SIP1** upon removal of capping moieties by photo irradiation.

In addition, DLS measurements revealed >90% decrease in scattering light intensities within 6 h after 30 min light irradiation (Figure 1e). In sharp contrast, without light irradiation, almost no change in scattering intensities was discernible within the same time range (inset in Figure 1e), confirming that ***h*SIP1** was intrinsically inert to spontaneous hydrolysis. Further, using a polarity-sensitive probe, Nile red, encapsulated within the hydrophobic core domain of ***h*SIP1**, phototriggered degradation of ***h*SIP1** was manifested by a pronounced decrease in the fluorescence emission of Nile red following 30 min light irradiation (Figure 1f). This indicated that Nile red was located in highly hydrophilic milieu upon triggered ***h*SIP1** degradation.

The rate of triggered fragmentation of SIPs plays a vital role considering their biomedical functions such as drug delivery. Presumably, the depolymerization rate could be modulated by the chemical structure, chain sequence, and topology of SIPs.[11b,c,21] To achieve adjustable release rates, two extra branching precursors, **M2** and **M3**, were utilized to fabricate photoresponsive ***h*SIP2** and ***h*SIP3**, possessing distinct core scaffolds but the same coronas as compared to ***h*SIP1**. After 30 min blue light irradiation, the release rate of ABA from ***h*SIP1** was faster than that of ***h*SIP2** (Figure 1g). This is in agreement with the stepwise depolymerization mechanism that the release of the *para* substituent via 1,6-elimination is more preferred than that of the *ortho* substituent via 1,4-elimination.[5d] Also, the depolymerization rate of ***h*SIP3** was slower than that of ***h*SIP1** as well (Figure 1g), possibly due to the slow generation of thiophenol. The chemical tuning of cascade fragmentation rates through structural modulation of *h*SIP scaffolds augurs the nature of programmed drug release. Most importantly, the self-immolative radial fragmentation feature of ***h*SIP1** can be retained when the capping moiety at the focal point was replaced with the reductive milieu-responsive disulfide-containing one (*SS*). For ***h*SIP4**, GSH-triggered cascade depolymerization was verified by triggered DOX release in a programmed manner, time-dependent decrease of scattering light intensity, and release of encapsulated Nile red probe into the aqueous milieu (Figure S9).

Next, blue light-induced intracellular release of DOX from ***h*SIP1** was *in situ* examined with HeLa cells by confocal laser scanning microscopy (CLSM). Upon coincubation without light irradiation, punctuated red-emitting dots of ***h*SIP1**-DOX were discernible inside cells, and most of them did not colocalize with LysoTracker green, which selectively stains late endosomes and lysosomes (Figure S10). Upon extending the incubation duration, the colocalization ratio between ***h*SIP1** red channel and LysoTracker green channel steadily decreased (Figure S10b), and the red channel emission intensity gradually increased (Figure S10c). This indicated that ***h*SIP1** species were increasingly taken up into cells and mainly located in the cytosol rather than in acidic organelles at extended incubation, possibly benefiting from the small size (~18 nm) and presence of cRGD targeting peptide segments at the periphery.[22] In addition, DOX red emission was not discernible in the cell nuclei even after 4 h coincubation without light irradiation, possibly due to the covalent binding nature of DOX (Figure S10).

To monitor intracellular light-triggered DOX release, a single HeLa cell after coincubation with ***h*SIP1** for 4 h was arbitrarily chosen and subjected to one scan of 458 nm argon laser irradiation. Upon extending the incubation time, punctuated red emissive dots from DOX gradually weakened and eventually disappeared, whereas continuously enhanced red emission in the cell nucleus appeared and colocalized well with acridine orange (AO), which selectively stains the cell nucleus (Figure 2a). This suggested that initially covalently conjugated

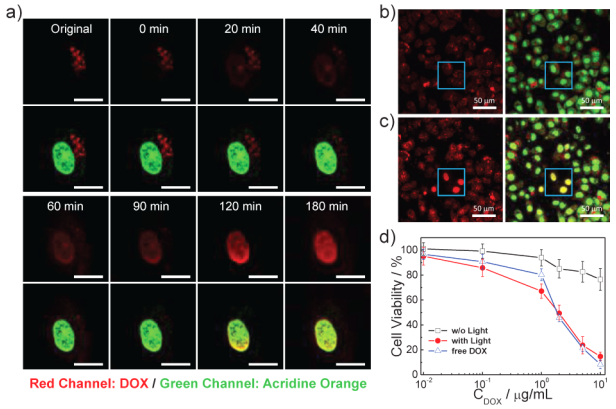

Figure 2. (a) Representative confocal laser scanning microscopy (CLSM, scar bar: 20 μm) images recorded for HeLa cells upon incubating for 0–180 min after one scan of 458 nm laser irradiation; top row, red channel images (DOX, 560 ± 20 nm); bottom row, overlay of red channel and green channel (acridine orange, 500 ± 20 nm) images. (b, c) CLSM images (scar bar: 50 μm) were recorded for HeLa cells subjected to further incubation for (b) 0 min and (c) 120 min after one scan of laser irradiation (458 nm) at the blue square box area; left row, red channel images (DOX, 560 ± 20 nm); right row, overlay of red channel and green channel (acridine orange, 500 ± 20 nm) images. (d) *In vitro* cytotoxicity determined by MTT assay against HeLa cells for aqueous solution of cRGD-decorated ***h*SIP1** without or with 30 min blue LED light irradiation (460 nm). In all cases, the cells were incubated with aqueous ***h*SIP1** solution for 4 h at first before blue light irradiation. Error bars represent mean ± SD, n = 4.

DOX was cleaved from the periphery of ***h*SIP1** upon 458 nm laser irradiation and entered into cell nucleus. Visible light-induced DOX release and subsequent nuclear entry were further studied on a larger scale under CLSM (Figure 2b,c), in which three cells in the square box were selectively irradiated by 458 nm argon laser for one scan. After further incubation for 120 min, continuous red emission of released DOX well-colocalized with AO-stained cell nuclei within the irradiation square area (Figure 2c). In contrast, for those cells outside the irradiation zone, discrete green and red emissions were clearly located in the cell nuclei and cytoplasm, respectively (Figure 2c). These results indicated that light irradiation triggered the depolymerization of ***h*SIP1**, and this is followed by DOX release at later stages and further diffusion into the cell nuclei, whereas intact ***h*SIP1** cannot efficiently enter into the nuclei. We can also conclude that intracellular drug release from *h*SIPs can be achieved in a spatiotemporal and programmed manner.

In vitro cytotoxicity of ***h*SIP1** was then examined via MTT assay against HeLa cells (Figure 2d). The cell viability of ***h*SIP1** without blue light irradiation exhibited negligible cytotoxicity up to a DOX equivalent concentration of 10 μg/mL. However, cell viability dramatically decreased to ~18% at a DOX equivalent concentration of 10 μg/mL when subjected to 30 min blue light irradiation. Note that control experiments using

DOI: 10.1021/jacs.5b05060
J. Am. Chem. Soc. 2015, 137, 11645–11655

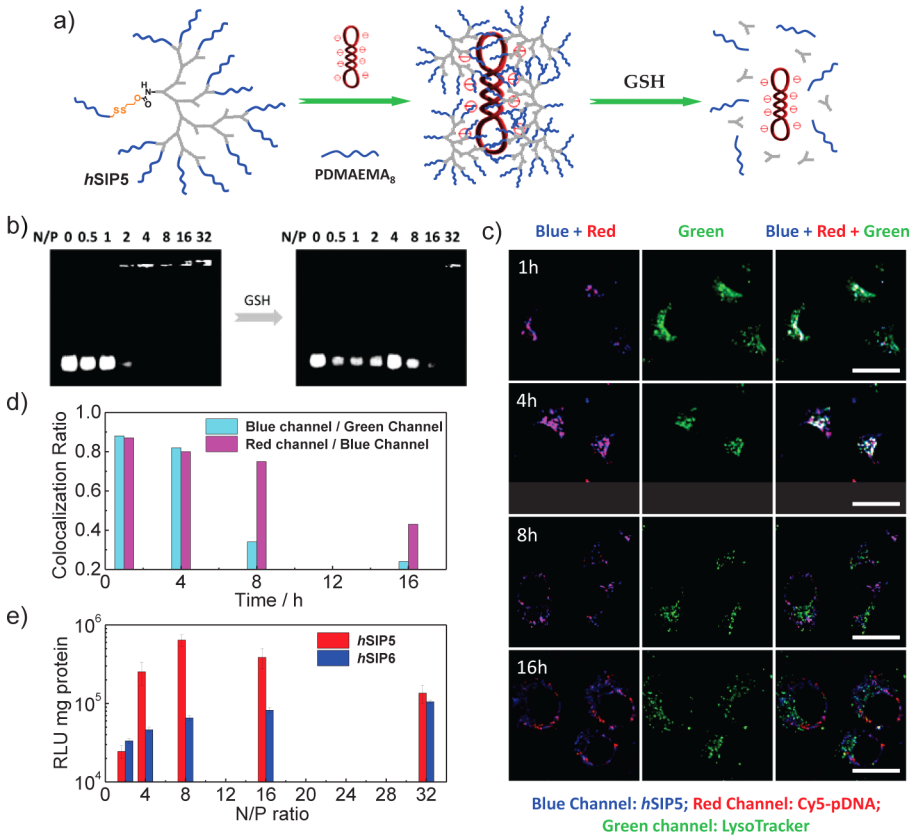

Figure 3. (a) Schematic illustration of the formation of electrostatic polyplexes between pDNA and ***h*SIP5** bearing multiple cationic PDMAEMA segments at the periphery; the subsequent ***h*SIP5** depolymerization and pDNA release was triggered by intracellular reductive milieu (e.g., GSH). (b) Gel electrophoresis analysis of pDNA mobility upon formation of electrostatic complexes with ***h*SIP5** at varying N/P ratios (left) before and (right) after treating with GSH. (c) Representative CLSM images (scar bar: 20 μm) of red (Cy5-pDNA, 670 ± 20 nm), green (LysoTracker, 520 ± 20 nm), and blue (*cou*-***h*SIP5**, 450 ± 20 nm) channels recorded for HeLa cells upon incubating with ***h*SIP5**/pDNA complex (N/P = 8) for varying periods. (d) Colocalization ratio analysis of blue channel to green channel and red channel to blue channel. (e) *In vitro* transfection efficiencies determined for polyplexes formed between luciferase-expressing pDNA and ***h*SIP5** or ***h*SIP6** at varying N/P ratios. Error bars represent mean ± SD, n = 4.

blue light irradiation alone did not apparently affect the cell viability. Except light-triggered release of DOX from ***h*SIP1**, degradation intermediates and products from the hyperbranched scaffold might also contribute to the observed cytotoxicity. We then conducted additional cell viability assays concerning the cytotoxicity of ***h*SIP4**-***h*SIP7** possessing inert or reductive/H_2O_2-cleavable capping moieties (Figure S11). It was found that nondegradable ***h*SIP6**, serving as a control, exhibited negligible cytotoxicity. Although DOX-loaded and disulfide-capped ***h*SIP4** exhibited potent cytotoxicity, ***h*SIP5** and ***h*SIP7** (capped with disulfide and boronic ester moieties, respectively) without peripherally conjugated drugs also exhibited cytotoxicity to some extent. The latter should be ascribed to self-immolative degradation intermediates (e.g., quinone methide) and products.[23] This poses a challenge toward their future *in vivo* drug delivery applications; however, upon appropriate chemical design, synergistic chemotherapy might also be achieved.[23]

Intracellular Reductive Milieu-Triggered pDNA Delivery by *h*SIPs Functionalized with Peripheral Cationic Segments. Apart from intracellular DOX delivery, we expect that *h*SIPs could be readily engineered into nonviral gene delivery vectors by replacing the peripheral chemotherapeutic DOX drug with cationic PDMAEMA segments. Intracellular pDNA release can be achieved by the elimination of multivalent interactions triggered by self-immolative degradation of cationic *h*SIP vectors (Figure 3a).[24] Installed with a disulfide-containing capping agent (*SS*) at the focal point, ***h*SIP5** with multiple cationic PDMAEMA in the periphery can effectively condense negatively charged pDNA via the formation of electrostatic polyplexes due to synergistic multivalent interactions, despite the fact that the $PDMAEMA_8$ homopolymer was deemed infeasible for efficient pDNA binding.[24b,c]

The formation of ***h*SIP5**/pDNA polyplexes was confirmed by TEM, zeta-potential, and DLS analysis, displaying increased size dimension and reversal of zeta potentials (Figure S12). In addition, complete gel retardation can be achieved at N/P ratios higher than 4 (Figure 3b). After treatment with 10 mM GSH, ***h*SIP5** underwent depolymerization due to cleavage of the disulfide bond and subsequent cascade radial fragmentation. Comparable to phototriggered ***h*SIP1** depolymerization (Figure 1d,e), GSH-actuated ***h*SIP5** degradation was also evidenced by a steady decrease of MW (Figure S13a). We surmised that GSH-triggered depolymerization of ***h*SIP5** should significantly attenuate pDNA binding capability, thereby unpacking the pDNA payload. As expected, after GSH addition, pDNA cannot be efficiently bound even at an N/P ratio as high as 16, as confirmed by gel electrophoresis analysis (Figure 3b). The disassociation of ***h*SIP5**/pDNA polyplexes upon treatment with 10 mM GSH was also evidenced by the substantially decreased

DOI: 10.1021/jacs.5b05060
J. Am. Chem. Soc. 2015, 137, 11645−11655

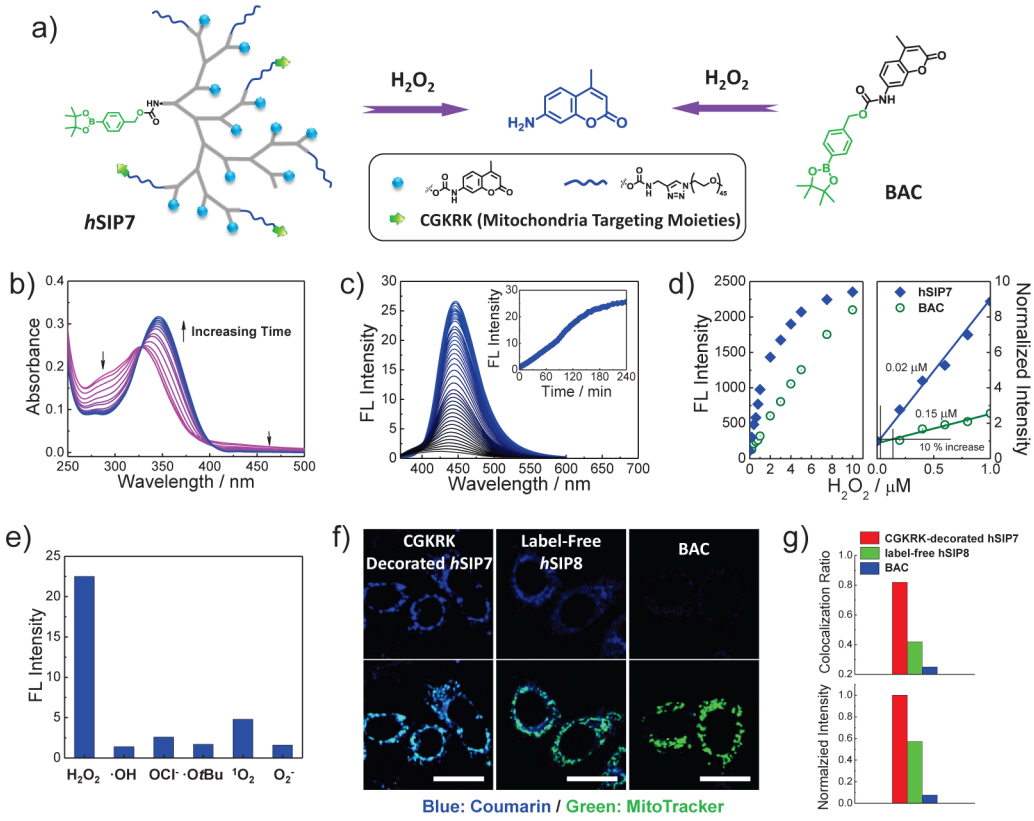

Figure 4. (a) Schematic illustration of H_2O_2-triggered self-immolative depolymerization of ***h*SIP7** possessing caged nonfluorescent AMC at the periphery; as a control, H_2O_2-triggered cleavage of small molecule **BAC** is also shown. Time-dependent (b) UV−vis absorbance spectra and (c) fluorescence emission spectra (λ_{ex} = 350 nm) recorded for the aqueous ***h*SIP7** solution (10 μM) upon incubating with H_2O_2 (100 μM) for varying time intervals (0−240 min); the inset in part c shows the evolution of emission intensity at 450 nm. (d) H_2O_2 concentration dependence of normalized emission intensities at 450 nm after incubating the aqueous solution of ***h*SIP7** (1 μM, containing 9 μM coumarin moieties) or **BAC** (9 μM) with H_2O_2 for 12 h. (e) Fluorescence response (λ_{ex} = 350 nm, λ_{em} = 450 nm) of ***h*SIP7** toward various ROS species. (f) Representative green channel (MitoTracker, 520 ± 20 nm) and blue channel (coumarin, 450 ± 20 nm) CLSM images (scar bar: 20 μm) recorded for HeLa cells upon incubating with CGKRK-decorated ***h*SIP7**, label-free ***h*SIP8**, and **BAC** for 12 h; the bottom row represents an overlay of blue and green channel images. (g) Colocalization ratio analysis between blue channel and green channel fluorescence, and normalized blue channel emission intensities quantified from CLSM images (f).

scattering light intensity and $\langle D_h \rangle$ upon extending incubation duration (Figure S13b).

With consideration of high cytoplasmic GSH concentration and reductive milieu in the cytosol, intracellular transfection efficiency of ***h*SIP5**/pDNA polyplexes (N/P = 8) was evaluated by taking advantage of cytoplasmic GSH-triggered pDNA release. By incubating polyplexes of coumarin-decorated ***h*SIP5** (*cou*-***h*SIP5**; Scheme S2) and Cy5-labeled pDNA (Cy5-pDNA) with HeLa cells for 1 h, most of the *cou*-***h*SIP5** blue emission overlapped with the red emission of Cy5-pDNA and LysoTracker Green emission, indicating that *cou*-***h*SIP5**/Cy5-pDNA polyplexes retained and mainly located within endolysosomes. Upon extending coincubation duration, the colocalization ratio between *cou*-***h*SIP5** blue emission and LysoTracker Green emission exhibited a pronounced decrease from 88% (1 h) to 34% (8 h) and 24% (16 h). Meanwhile, the colocalization ratio between *cou*-***h*SIP5** blue emission and Cy5-pDNA red emission remained ∼80% at 8 h coincubation, whereas it drastically decreased to ∼43% after 16 h coincubation (Figure 3c,d).

These results strongly suggested that cou-***h*SIP5**/Cy5-pDNA polyplexes underwent endosomal escape into the cytosol after 8 h incubation, and the complexes disassembled in the cytosol after being subjected to GSH-triggered ***h*SIP5** depolymerization and pDNA release. A quantitative assay of the transfection efficiency was performed using luciferase-expressing pDNA as the reporter gene (Figure 3e), and nondegradable ***h*SIP6**/pDNA complexes were employed as a control since cytoplasmic reductive milieu cannot cleave *Bn* functionality at the focal point. In the N/P range 4−32, *in vitro* gene transfection of ***h*SIP5**/pDNA polyplexes systematically presented higher efficiency than ***h*SIP6**/pDNA polyplexes, presumably due to the poor unpackaging efficacy for the latter. This conclusion was further verified by utilizing green fluorescent protein (GFP)-expressing pDNA as the reporter gene (Figure S14).

Mitochondria-Targeted Fluorescent Sensing of H_2O_2. In addition to spatiotemporal intracellular drug and gene delivery, we further explored the application scope of *h*SIPs and utilized them for intracellular fluorescent imaging and sensing. The focal point of ***h*SIP7** was caged with H_2O_2-responsive phenylboronic ester (*PB*); the periphery of ***h*SIP7** was dually functionalized with mitochondrion-targeting CGKRK peptide and AMC as caged fluorescent reporter. H_2O_2-triggered depolymerization of ***h*SIP7** was then conducted and monitored by GPC analysis (Figure S15). This process was accompanied by an evident bathochromic shift from 326 to 346 nm in the UV−vis spectra (Figure 4b) and a cumulative ∼25.5-fold

DOI: 10.1021/jacs.5b05060
J. Am. Chem. Soc. 2015, 137, 11645−11655

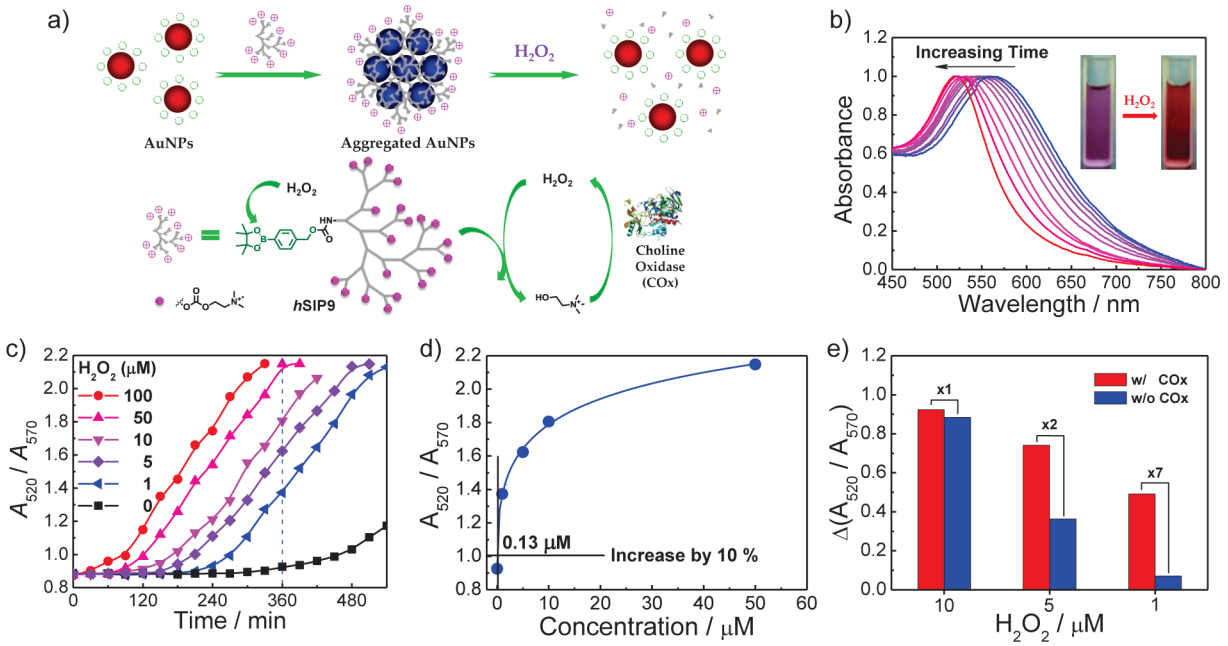

Figure 5. (a) Schematic illustration of the construction of colorimetric H_2O_2 sensing system by integrating negatively charged Au NPs with cationic ***h*SIP9** exhibiting H_2O_2-triggered cascade fragmentation and enzyme-mediated cycle amplification features. Time-dependent evolution of (b) UV−vis absorption spectra and (c) absorbance intensity ratios (A_{520}/A_{570}) recorded for the aqueous mixture of ***h*SIP9** (80 mg/L, 11 μM), Au NPs (80 mg/L), and COx (choline oxidase; 10 ng/mL) upon addition of H_2O_2. (d) H_2O_2 concentration dependence of absorbance intensity ratios (A_{520}/A_{570}) recorded for the aqueous mixture (80 mg/L ***h*SIP9**, 80 mg/mL Au NPs, 10 ng/mL COx) upon 6 h coincubation. (e) Absorbance intensity ratio shift, $\Delta(A_{520}/A_{570})$, recorded for the aqueous mixture (80 mg/L ***h*SIP9**, 80 mg/mL Au NPs) upon 6 h coincubation in the presence or absence of COx.

fluorescence emission increase within 240 min (Figure 4c). Compared with the small molecule control BAC (Figure S16), ***h*SIP7**-based H_2O_2 probe exhibited significant fluorescence emission increase and enhanced detection sensitivity (Figure 4d). Specifically, the detection limits (defined as 10% emission increase relative to the blank sample) toward H_2O_2 were determined to be ∼20 nM for ***h*SIP7** and ∼150 nM for **BAC**, which was in general agreement with the chemical amplification factor (∼9) of ***h*SIP7** (Figure 4d and Table 1). Moreover, the selectivity of ***h*SIP7**-based H_2O_2 probe over other reactive oxygen species (ROS) was well-retained due to the high specificity of phenylboronic ester toward H_2O_2 (Figure 4e). Thus, ***h*SIP7** can serve as a highly selective and sensitive fluorescent H_2O_2 probe. Another concern of ***h*SIP7**-based fluorescent H_2O_2 probe comes from batch-to-batch variation, leading to a discrepancy in chemical amplification factors and signal intensities. In preliminary experiments, we synthesized three additional batches of ***h*SIP7** in parallel. In the presence of excess H_2O_2, the overall fluorescence emission intensities remained almost constant (Figure S17). These results implied that batch-to-batch variations can be neglected to some extent.

Upon coincubating HeLa cells with CGKRK-decorated ***h*SIP7** for 12 h, strong punctuated AMC blue emissive dots were discerned inside cells, and most of them colocalized well with MitoTracker green (Figure 4f), whereas blue emission intensities originating from decaged AMC moieties of label-free ***h*SIP8** and **BAC** small molecules were only 57% and 7% relative to that of ***h*SIP7** (Figure 4f,g). These results confirmed that ***h*SIP7** decorated with CGKRK targeting peptide can efficiently find mitochondrion organelle, where phenylboronic ester capping agent was cleaved by endogenous H_2O_2 and ***h*SIP7** was subjected to depolymerization, thereby releasing AMC fluorophores and switching on the blue emission.

Colorimetric Detection of H_2O_2 by Integrating Enzyme-Directed Cycle Amplification with Au Nanoparticle Aggregates. Besides the intrinsic chemical amplification feature of *h*SIPs, the signal amplification performance could be further enhanced via rationally integrating with specific enzymatic reactions, in which released fragments could serve as enzymatic substrate and generate more substance capable of triggering depolymerization of *h*SIPs. Previously, Shabat et al.[25] originated the "dendritic chain reaction" principle to design a series of colorimetric and fluorescent probes solely based on SIDs of the first generation. We expected that *h*SIPs, possessing higher chemical amplification potency, installed with this cycle amplification module will enable ultrasensitive detection of specific substances. As a proof of concept, we fabricated an ultrasensitive colorimetric H_2O_2 detection system consisting of three components: negatively charged citric-acid-stabilized gold nanoparticles (AuNPs), CHO-labeled positively charged ***h*SIP9** capable of triggered fragmentation and CHO release upon H_2O_2 treating, and choline oxidase (COx) (Figure 5a).

H_2O_2-triggered generation of CHO from depolymerized ***h*SIP9** can be further oxidized by COx to generate more H_2O_2, which can in turn trigger the degradation of other unreacted ***h*SIP9** and release more CHO (Figure 5a). Upon addition of aqueous ***h*SIP9** solution (4−60 mg/L) into citrate-stabilized AuNP dispersion (∼8 nm in average diameter, 80 mg/L), the initial wine red color gradually turned purple blue and the UV−vis absorption peak red-shifted from ∼520 to ∼570 nm (Figure S18), indicating the formation of AuNP aggregates due to electrostatic interactions with ***h*SIP9**. However, when 9 equiv of H_2O_2 (relative to the phenylboronic ester caging moieties) was added to ***h*SIP9**/AuNP hybrid aggregates in the presence of COx, reversible color change from purple blue to wine red was

DOI: 10.1021/jacs.5b05060
J. Am. Chem. Soc. 2015, 137, 11645−11655

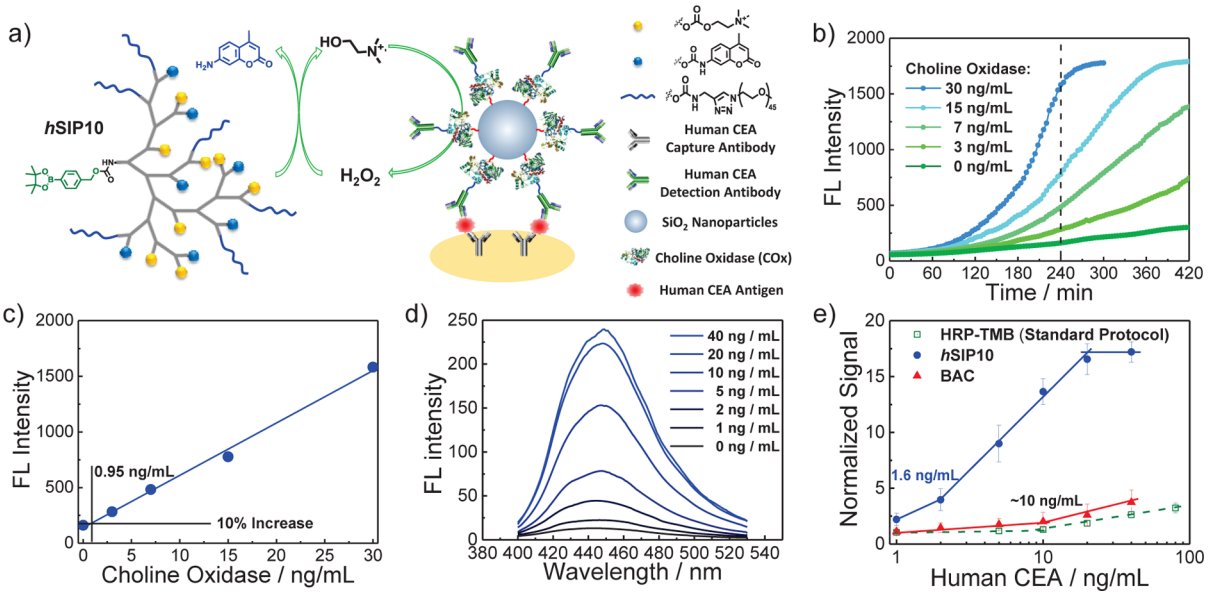

Figure 6. (a) Schematics of the construction of cycle signal amplification system from COx enzyme and ***h*SIP10** possessing caged nonfluorescent AMC and choline moieties at the periphery, which considerably improves the detection sensitivity of sandwich ELISA format toward human CEA. (b) Time-dependent emission intensity at 450 nm (λ_{ex} = 350 nm) recorded for the aqueous mixture of ***h*SIP10** (50 μM) and COx at varying concentrations upon addition of H_2O_2 (5 μM). (c) COx concentration dependence of emission intensities at 450 nm upon incubating the aqueous mixture for 4 h. (d) Fluorescence spectra and (e) human CEA concentration-dependent changes in emission intensities at 450 nm (λ_{ex} = 350 nm) obtained via the ELISA kit; surface captured SiNP-COx-ACEA (95/5 PBS/DMSO, pH 7.4, 37 °C) was coincubated with choline (2 μM) and ***h*SIP10** (10 μM, containing 25 μM coumarin moieties) or BAC (25 μM). As a control, the optical absorption at 450 nm was also recorded by following standard ELISA protocols using TMB (3,3′,5,5′-tetramethylbenzidine) as the HRP substrate. Error bars represent mean ± SD, n = 4.

achieved within ~330 min (Figure 5b), suggesting the disintegration of hybrid aggregates and formation of redispersed AuNPs. In addition, H_2O_2-triggered dispersion of AuNP aggregates can also be confirmed by TEM observations (Figure S19).

These promising preliminary results spurred us to further assess the H_2O_2-triggered signal amplification system in the presence of lower H_2O_2 concentrations. Upon H_2O_2 addition (0−100 μM), time-dependent evolutions of absorbance intensity ratios (A_{520}/A_{570}) were highly dependent on H_2O_2 levels (Figure 5c). The more H_2O_2 was added, the less time was needed to reach a plateau (i.e., complete depolymerization). Notably, when only ~0.1 equiv of H_2O_2 (1 μM) was introduced (relative to phenylboronic ester moieties), the time-dependent evolution of A_{520}/A_{570} revealed a sigmoidal shape, which was in accord with an autocatalytic process (Figure 5c). In contrast, in the absence of H_2O_2, ***h*SIP9**/AuNP hybrid aggregates were relatively stable, and there was no appreciable change in A_{520}/A_{570} ratios within ~6 h coincubation, although a slight increase can be still discerned after 9 h coincubation (Figure S20). Spontaneous hydrolysis of carbonate bonds to release CHO, which can generate H_2O_2 under COx enzymatic reaction, should account for the slight change in absorbance intensity ratio for the blank control. The H_2O_2 detection limit (defined as 10% A_{520}/A_{570} increase relative to the control) was determined to be ~0.13 μM after 360 min incubation (Figure 5d), which is more sensitive than that of the previously reported colorimetric H_2O_2 sensing system involving AuNPs.[17c] We also conducted supplementary experiments in the absence of COx (Figure 5e). The lack of positive feedback cycle amplification aided by enzymatic H_2O_2 generation led to a considerably decreased shift in absorbance intensity ratios, and this trend was more prominent at lower H_2O_2 levels (e.g., ~7 times difference at 1 μM H_2O_2).

Fluorescent H_2O_2 and Antigen Detection by Integrating with Enzyme-Directed Cycle Amplification and ELISA. Considering that the fluorescent H_2O_2 detection system integrated with enzyme-directed cycle amplification will possess more improved detection sensitivity, we further designed ***h*SIP10** bearing caged fluorescent AMC moieties at the periphery (Figure 6a). The time-dependent emission intensity changes at 450 nm recorded ***h*SIP10**-COx system in the presence of varying amount of H_2O_2 exhibited a sigmoidal trend. Importantly, 0.02 equiv of H_2O_2 (relative to phenylboronic ester moieties at the focal point) addition was capable of completely depolymerizing ***h*SIP10** if longer incubation duration was given (Figure S21). Further numerical fitting of reaction kinetics revealed that the process complied with the positive feedback cycle amplification model developed by the Shabat research group (Figure S21).[25b] These results verified that the coupling of intrinsic self-immolative chemical amplification with enzyme-mediated cycle amplification could significantly boost detection sensitivity.

Note that COx concentrations also affected the amplification efficacy of the ***h*SIP10**-COx system; therefore, it can be used for the detection of COx as well in the presence of a trace amount of H_2O_2 (e.g., 0.1 equiv relative to phenylboronic ester moieties). In this approach, the background signal could be minimized due to the fact that the ***h*SIP10**-COx system cannot amplify fluorescence signals without COx even if inadvertent hydrolysis will release CHO substrate. Upon gradually increasing COx levels (0−30 ng/mL), emission intensities at 450 nm of decaged AMC moieties from depolymerized ***h*SIP10** increased more abruptly (Figure 6b). Specifically, ***h*SIP10** was fully fragmented within ~300 min in the presence of 30 ng/mL COx (Figure 6b). When the incubation time was set at 240 min, the COx detection limit (defined as 10% AMC fluorescence emission increase relative to the blank control)

DOI: 10.1021/jacs.5b05060
J. Am. Chem. Soc. 2015, 137, 11645−11655

was determined to be ~0.95 ng/mL (Figure 6c), which is quite comparable to the antigen detection range of commercial ELISA kit.

Finally, we attempted to further explore functional applications of *h*SIPs in clinical diagnosis. As a proof-of-example, we fabricated an ELISA kit to detect human carcinoembryonic antigen (HCEA) by taking advantage of the cycle amplification capability of ***h*SIP10**. Toward this goal, COx and HCEA monoclonal antibody (ACEA) were covalently conjugated onto silica nanoparticles (SiNP-COx-ACEA) in a sequential manner (Scheme S3). All intermediate products and final SiNP-COx-ACEA hybrid nanoparticles were characterized by CLSM, UV−vis and fluorescence spectroscopy, and TEM measurements (Figures S22−S25). On the basis of the hydrolysis rate of BAC catalyzed by SiNP-COx-ACEA, the exact number of COx enzymes per SiNP was calculated to be ~5600 (Figure S22). Using the newly developed SiNP-COx-ACEA in combination with ***h*SIP10**, and following standard ELISA protocols, prominently increased fluorescence emission at 450 nm was discerned upon gradually increasing spiked CEA concentrations (Figure 6d). The CEA detection limit using ***h*SIP10**/SiNP-COx-ACEA system was determined to be 1.6 ng/mL, ~7 times better than that of BAC/SiNP-COx-ACEA or commercially available horseradish peroxidase (HRP)-3,3′,5,5′-tetramethyl-benzidine (TMB) assay (Figure 6e).[26]

CONCLUSIONS

A library of water-dispersible and multifunctionalized self-immolative polymers with a new type of hyperbranched chain topology, *h*SIPs, were synthesized by integrating one-pot polycondensation of three types of AB_2 precursors with sequential postfunctionalization. By rationally screening branching scaffolds, capping agents at the focal point, and peripheral functional groups and polymer segments, *h*SIPs with advanced drug/gene delivery and ultrasensitive detection functions were successfully constructed, exhibiting an intrinsic chemical amplification factor of up to 20 per *h*SIP molecule. The spontaneous radial depolymerization of *h*SIPs upon stimuli-triggered single cleavage of the capping moiety allowed for the construction of myriad functions including visible light-actuated intracellular release of conjugated chemotherapeutic drugs in a targeted and spatiotemporally controlled manner, intracellular delivery and cytoplasmic reductive milieu-mediated pDNA release, mitochondria-targeted fluorescent imaging and sensing of H_2O_2 with a high detection limit, and colorimetric H_2O_2 assay by integrating triggered dispersion of gold nanoparticle aggregates with enzyme-mediated cycle amplification. To further demonstrate the versatility and modularity of the *h*SIP platform, we constructed *h*SIP-based biosensors for the ultrasensitive detection of human carcinoembryonic antigen by coupling with enzyme-mediated positive feedback signal amplification and ELISA technique. The modular design, facile synthesis, multifunctional construction, water-dispersibility, high intrinsic chemical amplification, and potency of integrating with external cycle amplification modules of the reported *h*SIP platform opens a new avenue to fabricate novel stimuli-responsive materials with high selectivity, sensitivity, and specificity, a prerequisite for functions in complex biological media.

ASSOCIATED CONTENT

Supporting Information

The Supporting Information is available free of charge on the ACS Publications website at DOI: 10.1021/jacs.5b05060.

Detailed experimental procedures; NMR, UV−vis, FT-IR, MS, and fluorescence spectra; HPLC, GPC, and DLS data; and TEM and CLSM images (PDF)

AUTHOR INFORMATION

Corresponding Author

*sliu@ustc.edu.cn

Notes

The authors declare no competing financial interest.

ACKNOWLEDGMENTS

The financial support from the National Natural Scientific Foundation of China (NNSFC) Project (21274137, 51273190, 5147315, and 51033005) and Specialized Research Fund for the Doctoral Program of Higher Education (SRFDP, 20123402130010) is gratefully acknowledged.

REFERENCES

(1) Alberts, B.; Johnson, A.; Lewis, J.; Morgan, D.; Raff, M.; Roberts, K.; Walter, P. *Molecular Biology of the Cell*, 6th ed.; Garland Science: New York, 2014.

(2) (a) Zhu, L.; Anslyn, E. V. *Angew. Chem., Int. Ed.* **2006**, *45*, 1190−1196. (b) Wegst, U. G.; Bai, H.; Saiz, E.; Tomsia, A. P.; Ritchie, R. O. *Nat. Mater.* **2015**, *14*, 23−36. (c) Zhao, Y.; Sakai, F.; Su, L.; Liu, Y.; Wei, K.; Chen, G.; Jiang, M. *Adv. Mater.* **2013**, *25*, 5215−5256.

(3) (a) Alarcon, C. D. H.; Pennadam, S.; Alexander, C. *Chem. Soc. Rev.* **2005**, *34*, 276−285. (b) Roy, D.; Cambre, J. N.; Sumerlin, B. S. *Prog. Polym. Sci.* **2010**, *35*, 278−301. (c) Stuart, M. A. C.; Huck, W. T. S.; Genzer, J.; Muller, M.; Ober, C.; Stamm, M.; Sukhorukov, G. B.; Szleifer, I.; Tsukruk, V. V.; Urban, M.; Winnik, F.; Zauscher, S.; Luzinov, I.; Minko, S. *Nat. Mater.* **2010**, *9*, 101−113. (d) Liu, F.; Urban, M. W. *Prog. Polym. Sci.* **2010**, *35*, 3−23. (e) Spruell, J. M.; Hawker, C. J. *Chem. Sci.* **2011**, *2*, 18−26. (f) Wang, Y.; Byrne, J. D.; Napier, M. E.; DeSimone, J. M. *Adv. Drug Delivery Rev.* **2012**, *64*, 1021−1030. (g) Blum, A. P.; Kammeyer, J. K.; Rush, A. M.; Callmann, C. E.; Hahn, M. E.; Gianneschi, N. C. *J. Am. Chem. Soc.* **2015**, *137*, 2140−2154.

(4) (a) Hu, J. M.; Liu, S. Y. *Macromolecules* **2010**, *43*, 8315−8330. (b) Ge, Z. S.; Liu, S. Y. *Chem. Soc. Rev.* **2013**, *42*, 7289−7325. (c) Hu, J. M.; Liu, S. Y. *Acc. Chem. Res.* **2014**, *47*, 2084−2095. (d) Hu, J. M.; Zhang, G. Y.; Ge, Z. S.; Liu, S. Y. *Prog. Polym. Sci.* **2014**, *39*, 1096−1143.

(5) (a) Amir, R. J.; Zhong, S.; Pochan, D. J.; Hawker, C. J. *J. Am. Chem. Soc.* **2009**, *131*, 13949−13951. (b) Raghupathi, K. R.; Azagarsamy, M. A.; Thayumanavan, S. *Chem. - Eur. J.* **2011**, *17*, 11752−11760. (c) Hu, J. M.; Zhang, G. Q.; Liu, S. Y. *Chem. Soc. Rev.* **2012**, *41*, 5933−5949. (d) Samarajeewa, S.; Shrestha, R.; Li, Y. L.; Wooley, K. L. *J. Am. Chem. Soc.* **2012**, *134*, 1235−1242. (e) Rao, J. Y.; Hottinger, C.; Khan, A. *J. Am. Chem. Soc.* **2014**, *136*, 5872−5875. (f) Ding, Y.; Kang, Y. T.; Zhang, X. *Chem. Commun.* **2015**, *51*, 996−1003. (g) Rosenbaum, I.; Harnoy, A. J.; Tirosh, E.; Buzhor, M.; Segal, M.; Frid, L.; Shaharabani, R.; Avinery, R.; Beck, R.; Amir, R. J. *J. Am. Chem. Soc.* **2015**, *137*, 2276−2284.

(6) (a) Amir, R. J.; Pessah, N.; Shamis, M.; Shabat, D. *Angew. Chem., Int. Ed.* **2003**, *42*, 4494−4499. (b) de Groot, F. M.; Albrecht, C.; Koekkoek, R.; Beusker, P. H.; Scheeren, H. W. *Angew. Chem., Int. Ed.* **2003**, *42*, 4490−4494. (c) Szalai, M. L.; Kevwitch, R. M.; McGrath, D. V. *J. Am. Chem. Soc.* **2003**, *125*, 15688−15689. (d) McGrath, D. V. *Mol. Pharmaceutics* **2005**, *2*, 253−263. (e) Amir, R. J.; Shabat, D. *Adv. Polym. Sci.* **2006**, *192*, 59−94. (f) Shabat, D. *J. Polym. Sci., Part A: Polym. Chem.* **2006**, *44*, 1569−1578. (g) Gingras, M.; Raimundo, J. M.;

DOI: 10.1021/jacs.5b05060
J. Am. Chem. Soc. 2015, 137, 11645−11655

Chabre, Y. M. *Angew. Chem., Int. Ed.* **2007**, *46*, 1010−1017. (h) Avital-Shmilovici, M.; Shabat, D. *Soft Matter* **2010**, *6*, 1073. (i) Ramireddy, R. R.; Raghupathi, K. R.; Torres, D. A.; Thayumanavan, S. *New J. Chem.* **2012**, *36*, 340−349. (j) Leiro, V.; Garcia, J. P.; Tomas, H.; Pego, A. P. *Bioconjugate Chem.* **2015**, *26*, 1182−1197.

(7) (a) Sagi, A.; Weinstain, R.; Karton, N.; Shabat, D. *J. Am. Chem. Soc.* **2008**, *130*, 5434−5435. (b) Blencowe, C. A.; Russell, A. T.; Greco, F.; Hayes, W.; Thornthwaite, D. W. *Polym. Chem.* **2011**, *2*, 773−790. (c) Esser-Kahn, A. P.; Odom, S. A.; Sottos, N. R.; White, S. R.; Moore, J. S. *Macromolecules* **2011**, *44*, 5539−5553. (d) Peterson, G. I.; Larsen, M. B.; Boydston, A. J. *Macromolecules* **2012**, *45*, 7317−7328. (e) Wong, A. D.; DeWit, M. A.; Gillies, E. R. *Adv. Drug Delivery Rev.* **2012**, *64*, 1031−1045. (f) Gnaim, S.; Shabat, D. *Acc. Chem. Res.* **2014**, *47*, 2970−2984. (g) Phillips, S. T.; DiLauro, A. M. *ACS Macro Lett.* **2014**, *3*, 298−304. (h) Phillips, S. T.; Robbins, J. S.; DiLauro, A. M.; Olah, M. G. *J. Appl. Polym. Sci.* **2014**, *131*, 40992.

(8) (a) Patri, A. K.; Majoros, I. J.; Baker, J. R. *Curr. Opin. Chem. Biol.* **2002**, *6*, 466−471. (b) Rolland, O.; Turrin, C. O.; Caminade, A. M.; Majoral, J. P. *New J. Chem.* **2009**, *33*, 1809−1824.

(9) (a) Bosman, A. W.; Janssen, H. M.; Meijer, E. W. *Chem. Rev.* **1999**, *99*, 1665−1688. (b) Tomalia, D. A.; Frechet, J. M. J. *J. Polym. Sci., Part A: Polym. Chem.* **2002**, *40*, 2719−2728.

(10) (a) Dewit, M. A.; Gillies, E. R. *J. Am. Chem. Soc.* **2009**, *131*, 18327−18334. (b) de Gracia Lux, C.; McFearin, C. L.; Joshi-Barr, S.; Sankaranarayanan, J.; Fomina, N.; Almutairi, A. *ACS Macro Lett.* **2012**, *1*, 922−926. (c) Esser-Kahn, A. P.; Sottos, N. R.; White, S. R.; Moore, J. S. *J. Am. Chem. Soc.* **2010**, *132*, 10266−10268. (d) McBride, R. A.; Gillies, E. R. *Macromolecules* **2013**, *46*, 5157−5166. (e) Zhang, L.-J.; Deng, X.-X.; Du, F.-S.; Li, Z.-C. *Macromolecules* **2013**, *46*, 9554−9562. (f) Peterson, G. I.; Church, D. C.; Yakelis, N. A.; Boydston, A. J. *Polymer* **2014**, *55*, 5980−5985.

(11) (a) Zhang, H.; Yeung, K.; Robbins, J. S.; Pavlick, R. A.; Wu, M.; Liu, R.; Sen, A.; Phillips, S. T. *Angew. Chem., Int. Ed.* **2012**, *51*, 2400−2404. (b) Yeung, K.; Kim, H.; Mohapatra, H.; Phillips, S. T. *J. Am. Chem. Soc.* **2015**, *137*, 5324−5327. (c) DiLauro, A. M.; Lewis, G. G.; Phillips, S. T. *Angew. Chem., Int. Ed.* **2015**, *54*, 6200−6205. (d) DiLauro, A. M.; Abbaspourrad, A.; Weitz, D. A.; Phillips, S. T. *Macromolecules* **2013**, *46*, 3309−3313. (e) Fan, B.; Trant, J. F.; Wong, A. D.; Gillies, E. R. *J. Am. Chem. Soc.* **2014**, *136*, 10116−10123. (f) Peterson, G. I.; Boydston, A. J. *Macromol. Rapid Commun.* **2014**, *35*, 1611−1614.

(12) (a) Weinstain, R.; Sagi, A.; Karton, N.; Shabat, D. *Chem. - Eur. J.* **2008**, *14*, 6857−6861. (b) Weinstain, R.; Baran, P. S.; Shabat, D. *Bioconjugate Chem.* **2009**, *20*, 1783−1791.

(13) Liu, G. H.; Wang, X. R.; Hu, J. M.; Zhang, G. Y.; Liu, S. Y. *J. Am. Chem. Soc.* **2014**, *136*, 7492−7497.

(14) (a) Hawker, C. J.; Lee, R.; Frechet, J. M. J. *J. Am. Chem. Soc.* **1991**, *113*, 4583−4588. (b) Hawker, C. J.; Frechet, J. M. J. *Polymer* **1992**, *33*, 1507−1511. (c) Uhrich, K. E.; Hawker, C. J.; Frechet, J. M. J.; Turner, S. R. *Macromolecules* **1992**, *25*, 4583−4587. (d) Spindler, R.; Frechet, J. M. J. *Macromolecules* **1993**, *26*, 4809−4813. (e) Kim, Y. H.; Webster, O. W. *J. Am. Chem. Soc.* **1990**, *112*, 4592−4593.

(15) (a) Wooley, K. L.; Du, W. J.; Nystrom, A. M.; Zhang, L.; Powell, K. T.; Li, Y. L.; Cheng, C.; Wickline, S. A. *Biomacromolecules* **2008**, *9*, 2826−2833. (b) Imbesi, P. M.; Gohad, N. V.; Eller, M. J.; Orihuela, B.; Rittschof, D.; Schweikert, E. A.; Mount, A. S.; Wooley, K. L. *ACS Nano* **2012**, *6*, 1503−1512. (c) Pollack, K. A.; Imbesi, P. M.; Raymond, J. E.; Wooley, K. L. *ACS Appl. Mater. Interfaces* **2014**, *6*, 19265−19274.

(16) (a) Gao, C.; Yan, D. *Prog. Polym. Sci.* **2004**, *29*, 183−275. (b) Wang, D.; Zhao, T.; Zhu, X.; Yan, D.; Wang, W. *Chem. Soc. Rev.* **2015**, *44*, 4023−4071.

(17) (a) Hu, X. L.; Hu, J. M.; Tian, J.; Ge, Z. S.; Zhang, G. Y.; Luo, K. F.; Liu, S. Y. *J. Am. Chem. Soc.* **2013**, *135*, 17617−17629. (b) Wang, X. R.; Liu, G. H.; Hu, J. M.; Zhang, G. Y.; Liu, S. Y. *Angew. Chem., Int. Ed.* **2014**, *53*, 3138−3142. (c) Li, C. H.; Hu, J. M.; Liu, T.; Liu, S. Y. *Macromolecules* **2011**, *44*, 429−431. (d) Li, C. H.; Wu, T.; Hong, C. Y.; Zhang, G. Q.; Liu, S. Y. *Angew. Chem., Int. Ed.* **2012**, *51*, 455−459.

(18) Hu, X. L.; Liu, G. H.; Li, Y.; Wang, X. R.; Liu, S. Y. *J. Am. Chem. Soc.* **2015**, *137*, 362−368.

(19) (a) Carl, P. L.; Chakravarty, P. K.; Katzenellenbogen, J. A. *J. Med. Chem.* **1981**, *24*, 479−480. (b) de Groot, F. M. H.; Loos, W. J.; Koekkoek, R.; van Berkom, L. W. A.; Busscher, G. F.; Seelen, A. E.; Albrecht, C.; de Bruijn, P.; Scheeren, H. W. *J. Org. Chem.* **2001**, *66*, 8815−8830. (c) Warnecke, A.; Kratz, F. *J. Org. Chem.* **2008**, *73*, 1546−1552. (d) Alouane, A.; Labruère, R.; Le Saux, T.; Schmidt, F.; Jullien, L. *Angew. Chem., Int. Ed.* **2015**, *54*, 7492−7509.

(20) Zhang, Y. F. Fabrication of Supramolecular Assemblies and Functional Materials Based on Responsive Polymers. Ph.D. Thesis, University of Science and Technology of China, Hefei, China, May 2010.

(21) (a) Olejniczak, J.; Chan, M.; Almutairi, A. *Macromolecules* **2015**, *48*, 3166−3172. (b) Robbins, J. S.; Schmid, K. M.; Phillips, S. T. *J. Org. Chem.* **2013**, *78*, 3159−3169.

(22) Kagaya, H.; Oba, M.; Miura, Y.; Koyama, H.; Ishii, T.; Shimada, T.; Takato, T.; Kataoka, K.; Miyata, T. *Gene Ther.* **2012**, *19*, 61−69.

(23) Noh, J.; Kwon, B.; Han, E.; Park, M.; Yang, W.; Cho, W.; Yoo, W.; Khang, G.; Lee, D. *Nat. Commun.* **2015**, *6*, 6907.

(24) (a) Pack, D. W.; Hoffman, A. S.; Pun, S.; Stayton, P. S. *Nat. Rev. Drug Discovery* **2005**, *4*, 581−593. (b) Layman, J. M.; Ramirez, S. M.; Green, M. D.; Long, T. E. *Biomacromolecules* **2009**, *10*, 1244−1252. (c) van de Wetering, P.; Cherng, J. Y.; Talsma, H.; Crommelin, D. J. A.; Hennink, W. E. *J. Controlled Release* **1998**, *53*, 145−153.

(25) (a) Sella, E.; Shabat, D. *J. Am. Chem. Soc.* **2009**, *131*, 9934−9936. (b) Sella, E.; Lubelski, A.; Klafter, J.; Shabat, D. *J. Am. Chem. Soc.* **2010**, *132*, 3945−3952. (c) Perry-Feigenbaum, R.; Sella, E.; Shabat, D. *Chem. - Eur. J.* **2011**, *17*, 12123−12128.

(26) de la Rica, R.; Stevens, M. M. *Nat. Nanotechnol.* **2012**, *7*, 821−824.

DOI: 10.1021/jacs.5b05060
J. Am. Chem. Soc. 2015, 137, 11645−11655